RSC Chemical Biology

ROYAL SOCIETY OF CHEMISTRY

PAPER

View Article Online
View Journal | View Issue

Cite this: *RSC Chem. Biol.*, 2026, 7, 708

Chemical modulation of the unfolded protein response reveals an antiviral role for the PERK pathway in human coronavirus 229E infection

Isabella E. Pellizzari-Delano, Trinity H. Tooley, Debanjana Mondal, Keya Jani, Carla E. Gallardo-Flores and Che C. Colpitts *

Broad spectrum antivirals are critical to respond rapidly to the threat posed by newly emerging RNA viruses. One potential candidate is the natural compound thapsigargin (Tg). Tg potently induces endoplasmic reticulum (ER) stress and activates the unfolded protein response (UPR). Recent studies have demonstrated that Tg has robust antiviral activity against several human coronaviruses (CoVs), including SARS-CoV-2, although the specific antiviral mechanism(s) have remained unclear. Here, we aimed to characterize the role of the UPR in the antiviral activity of Tg against HCoV-229E, a model common cold CoV. Consistent with previous findings, we show that a short 30-minute priming of A549 cells with Tg potently inhibits HCoV-229E infection. Time-of-addition assays showed that Tg is most effective when added up to 8 hours post-infection. Furthermore, Tg inhibits the accumulation of double-stranded RNA in infected cells, suggesting that Tg inhibits early stages of viral RNA replication. Using selective UPR pathway inhibitors to narrow down the role of these pathways in mediating the antiviral effect of Tg, we show that the inhibition of IRE1 or ATF6 does not impair the ability of Tg to inhibit HCoV-229E infection. The use of stable knockdown A549 cells in which IRE1, PERK, or ATF6 expression was silenced further revealed that the antiviral activity of Tg is not dependent on the expression of any of the three UPR sensors individually. However, HCoV-229E replication is inhibited in A549-shIRE1 cells, or in cells treated with the IRE1 inhibitor (KIRA6), suggesting that IRE1 activation may play a pro-viral role during HCoV-229E infection. Selective UPR pathway activators were used to further probe down the role of each pathway during HCoV-229E infection. Activation of the PERK pathway, but not IRE1 or ATF6 pathways, inhibits HCoV-229E infection. Lastly, to more broadly test the antiviral role of PERK against CoV RNA replication, we used BHK-21 cells that stably express a SARS-CoV-2 replicon. We show that PERK activation inhibits SARS-CoV-2 replication similarly to Tg. Overall, these findings provide insight into the antiviral mechanism(s) of Tg against CoV infection and demonstrate that modulation of the UPR may be exploited as an antiviral strategy.

Received 19th September 2025,
Accepted 24th February 2026

DOI: 10.1039/d5cb00242g

rsc.li/rsc-chembio

Introduction

Five years after the beginning of the COVID-19 pandemic, the significant global health threat posed by newly emerging viruses is still concerning. Although the COVID-19 pandemic demonstrated that effective vaccines and antiviral drugs can be developed for a newly emerging virus, there is a need for broadly acting, host-centric antiviral drugs that could be readily deployed in the context of a future, novel emergence event. Antivirals that do not target specific viral proteins, but rather function by enhancing host antiviral responses, are advantageous as they are expected to have broad antiviral activity and a high barrier to resistance.[1] One such compound that exhibits broad spectrum antiviral activity is thapsigargin (Tg).

Recent literature has demonstrated the broad-spectrum antiviral activity of Tg, a natural product isolated from the Mediterranean plant, *Thapsia garganica*. Indeed, Tg possesses robust and broadly acting antiviral activity against human coronaviruses (CoVs), including endemic viruses such as HCoV-229E and HCoV-OC43, as well as the highly pathogenic MERS-CoV and SARS-CoV-2.[2,3] Tg potently inhibits the replication of HCoV-229E, as marked by a reduction in the levels of viral non-structural proteins (nsp) 8 and 12, key components of the viral replication complex.[3] Interestingly, while both Tg and HCoV-229E infection induce ER stress in Huh7 cells, Tg-induced ER stress was proposed to reverse CoV-mediated inhibition of stress response factors, thereby protecting against

Department of Biomedical and Molecular Sciences, Queen's University, Kingston, ON K7L 3N6, Canada. E-mail: che.colpitts@queensu.ca

infection.[3] Furthermore, Tg has been shown to inhibit the replication of other major respiratory viruses, including respiratory syncytial virus (RSV) and influenza A virus (IAV),[4] in which the antiviral effect of Tg against IAV was accompanied by enhanced host antiviral interferon responses.

Tg is a well-known inhibitor of the sarcoplasmic/endoplasmic reticulum (ER) Ca^{2+} ATPase (SERCA) pump,[5] which plays a critical role in regulating Ca^{2+} homeostasis across the cell cytoplasm and ER lumen. Inhibition of SERCA by Tg depletes Ca^{2+} stores within the ER, inducing ER stress and the unfolded protein response (UPR).[5] The UPR is a highly conserved mammalian response pathway that transcriptionally upregulates genes that function to restore proteostasis, or, under periods of intense and prolonged stress, induce cellular apoptosis.[6] The UPR is comprised of three signalling pathways, each regulated upstream by the activation of a corresponding transmembrane ER resident sensor/receptor, namely inositol requiring protein 1 (IRE1), PKR-like endoplasmic reticulum kinase (PERK), and activating transcription factor 6 (ATF6).[6] The endonuclease activity of IRE1 mediates the unconventional splicing of target gene X binding protein 1 (XBP1). This splicing event generates a frameshift variant known as XBP1 spliced (XBP1s) that functions as a potent transcription factor that upregulates genes that promote protein folding and ER-associated degradation.[7] Activation of PERK leads to the phosphorylation of eukaryotic translation initiation factor 2α (eIF2α), which temporarily halts global cap-dependent translation, limiting the synthesis of new proteins entering the ER.[8] Phosphorylation of eIF2α mediates the activation of activating transcription factor 4 (ATF4), which controls the expression of genes involved in alleviating ER stress, or inducing apoptosis, such as including CCAAT-enhancer-binding protein homologous protein (CHOP).[9,10] Lastly, following activation, ATF6 translocates to the Golgi, where it is proteolytically cleaved to reveal its NH_2 domain, also known as ATF6-N.[11] ATF6-N also functions as a transcription factor that upregulates the expression of genes involved in restoring proteostasis.[11]

One hypothesis is that UPR activation mediates the antiviral effect of Tg. However, the exact antiviral mechanism(s) of Tg against CoVs remains unclear, and the role of specific UPR pathways in mediating the antiviral activity of Tg is not well understood. In this work, we sought to better understand the antiviral mechanism of Tg against the model common cold CoV HCoV-229E by characterizing which branches of the UPR modulate HCoV-229E infection and could mediate the antiviral effect of Tg. Expanding on the findings of Shaban *et al.* that Tg inhibits HCoV-229E infection,[3] we have shown that Tg is most effective when added up to 8 hours post infection, suggesting that Tg treatment inhibits an early post-entry step of the viral replication cycle, such as viral protein expression or RNA synthesis. Activation of all three UPR pathways is expedited in cells primed with Tg. Additionally, chemical modulation of the UPR during infection using selective small molecule activators and inhibitors suggests that activation of the PERK pathway is antiviral against both HCoV-229E and SARS-CoV-2 RNA replication. On the other hand, inhibition of IRE1 strongly inhibited HCoV-229E infection, reflecting a proviral role for the IRE1 pathway. We show that genetic silencing of IRE1, ATF6, or PERK expression does not impair the antiviral activity of Tg, suggesting that none of the UPR pathways are individually responsible for the antiviral effect of Tg. Overall, these findings demonstrate that pharmacological modulation of the UPR during infection may provide a host-centric antiviral strategy and provide insight into the antiviral mechanism of Tg against human CoV infection.

Methods

Cells and viruses

Parental A549 cells (NR-52268) were obtained from the NIAID-funded Biodefence and Emerging Infections (BEI) Resources Repository and were cultured in Ham's F-12 K (Kaighn's) medium (Fisher Scientific #21127030) supplemented with 10% fetal bovine serum (FBS) and 1% penicillin/streptomycin (pen/strep). Huh7 cells (JCRB0403) were obtained from the Japanese Collection of Research Bioresources Cell Bank. 293T/17 (CRL-11268) cells were obtained from the American Type Culture Collection. Huh7 and 293T/17 cells were cultured in Dulbecco's modified Eagle medium (DMEM; ThermoFisher #11995065) supplemented with 10% FBS and 1% pen/strep. BHK-21 SARS-CoV-2-Rep-NanoLuc-Neo cells[12] were obtained from the BEI Resources Repository (NR-58876), and cultured in DMEM supplemented with 10% FBS, 1% pen/strep, and 200 μg mL^{-1} of G418 (ThermoFisher #10131027). HCoV-229E was obtained from the BEI Resources Repository (NR-52726) and propagated on Huh7 cells as previously described.[13] Unless otherwise stated, HCoV-229E-infected cells were incubated at 33 °C.

UPR inhibitors and activators

Thapsigargin (Tg) was kindly provided by Dr Andrew Evans (Queen's University) or purchased from Thermo Scientific (T7458). AA147 (E0745), IXA4 (S9797), CeapinA7 (E1099) and KIRA6 (S8658) were purchased from Selleckchem. CCT020312 (324879) and GSK2606414 (516535) were purchased from Sigma-Aldrich. Stocks were prepared in dimethyl sulfoxide (DMSO), which was used as the vehicle control.

Plasmids

Lentiviral pLKO.1-shATF6, pLKO.1-shIRE1 and pLKO.1-shPERK constructs were kindly provided by Dr Craig McCormick (Dalhousie University, Canada). For production of lentivirus, psPAX2 (#12260) and VSV-G (# 8454) were obtained from Addgene.

Generation of stable cell lines

To produce lentivirus, 293T/17 cells were seeded in a 6-well plate at 8×10^5 cells per well overnight. The next day, transfection mixes were prepared as followed: 600 ng psPAX2 packaging plasmid, 800 ng pLKO.1 transfer plasmid and 600 ng VSV-G envelope plasmid and 6 μL of lipofectamine 2000. Supernatants

were harvested 48- and 72-hours post transfection and lentiviruses were filtered using a 0.45 μm filter. For the generation of shCTRL, shATF6, shIRE1 and shPERK cell lines, A549 cells were seeded in a 6-well plate at a density of 2×10^5 cells per well overnight and subsequently transduced with lentivirus in the presence of 8 μg mL^{-1} of polybrene. Transduced cells were selected at 72 hours post transduction in either 3 μg mL^{-1} puromycin or 10 μg mL^{-1} blasticidin. Successful knockdown was confirmed by western blot analysis.

Antibodies

Primary antibodies against IRE1α (Cell Signaling Technology (CST) 3294, dilution 1 : 1000), ATF6 (CST 8089, dilution 1 : 1000), PERK (CST 5683, dilution 1 : 1000), XBP1s (CST 12782T, dilution 1 : 1000), HERPUD1 (Abcam ab150424, dilution 1 : 1000), HCoV-229E N (SinoBiological 40640-T62, dilution 1 : 10 000), beta-actin (Abcam ab8226, dilution 1 : 5000), alpha-tubulin (Thermo Scientific MA5-31466, dilution 1 : 5000), and GAPDH (Thermo Scientific MA5-15738, dilution 1 : 1000) were used for western blotting. The secondary antibodies Licor IRDye-680 (red) goat anti-mouse and IRDye-800 (green) goat anti-rabbit were also used. For immunofluorescence (IF), cells were stained using antibodies against calnexin (Sigma C4731, dilution 1 : 200) or dsRNA (Kerafast ES2001, dilution 1 : 65), followed by AlexaFluor-488 (CST 4408S or 4412S) or AlexaFluor-555 (CST 8890S or 8889S) conjugated secondary antibodies diluted 1 : 1000.

Western blot

Protein was extracted from cell lysates using Laemmli buffer (12.5 mM Tris–HCl (pH 6.8), 4% SDS, 20% glycerol) supplemented with ETDA, protease and phosphatase inhibitors. Cell lysates were sheared using QIAshredder columns (QIAGEN, 79654). Samples were separated by SDS-PAGE and transferred to nitrocellulose membranes using the TransBlot Turbo System (Bio-Rad) as per the manufacturer protocol. Membranes were blocked in 5% milk dissolved in 1X TBS-T (Tris-buffered saline with 0.1% Tween-20) for 1 hour. Primary antibodies were diluted in blocking buffer and were incubated at 4 °C overnight. The next morning, membranes were washed with 1X TBS-T and then incubated at room temperature for 1 hour with secondary antibodies diluted 1 : 10 000 in blocking buffer. Membranes were then washed with 1X TBS-T followed by 1X TBS and imaged using a Licor Odyssey® Clx imager.

RT-qPCR

Cellular RNA was isolated from cellular lysates using the Monarch Total RNA Miniprep Kit (New England Biolabs) or Qiagen RNAeasy kit as per the manufacturer's protocol. Extracted RNA was reverse transcribed to generate cDNA using the High-Capacity cDNA Synthesis Kit (Thermo Scientific). Quantitative PCR (qPCR) was performed using the PowerTrack™ SYBR Green Master Mix (Thermo Scientific) with specific primers outlined in Table 1. Viral and cellular gene expression was normalized to cellular actin using the $2^{-\Delta C_t}$ method.

Luciferase assays

Luciferase reporter activity in the BHK-CoV-2 replicon cells was measured using the NanoFuel® GLOW Assay for Oplophorus Luciferases from NanoLight Technology (Cat# 325). The NanoFuel® GLOW Reagent was brought to room temperature and 20 μL of 50× Oplo-GLOW Substrate was added to 1 mL of NanoFuel® GLOW Reagent. Once mixed, equal volume of the reagent-substrate mixture was added (100 μL in a 96-well plate) to each well containing 100 μL of media. The plate was incubated for 5 minutes after which the cells were scraped and transferred to a white flat-bottom 96-well plate for measurement using a Promega GloMax. For measurement of HCoV-229E Renilla luciferase reporter activity, 50 μL of prepared 1 mg mL^{-1} coelenterazine substrate (NanoLight) was injected into white plates containing 20 μL of cell lysate and measured by Promega GloMax.

Immunofluorescence

A549 or BHK-CoV-2 replicon cells were seeded on coverslips in a 12-well plate at a density of 2×10^5 cells per well and incubated overnight. A549 cells were subsequently infected with HCoV-229E at a multiplicity of infection (MOI) of 0.5 plaque-forming units (PFU)/cell for 24 hours. Cells were fixed in 10% formalin for 1 hour at room temperature. Fixed samples were permeabilized with 0.1% Triton-X 100 and blocked in PBS containing 5% FBS solution for 1 hour. Cells were stained for calnexin or dsRNA, followed by staining with AlexaFluor-488 or AlexaFluor-

Table 1 Oligos used in this study

Target	Forward primer (5′–3′)	Reverse primer (5′–3′)
Actin (housekeeping)	CTGGGAGTGGGTGGAGGC	TCAACTGGTCTCAAGTCAGTG
18s rRNA (housekeeping)	TTCGAACGTCTGCCCTATCAA	GATGTGGTAGCCGTTTCTCAGG
HCoV-229E N	AGGCGCAAGAATTCAGAACCAGAG	AGCAGGACTCTGATTACGAGAAAG
BiP	GCCTGTATTTCTAGACCTGCC	TTCATCTTGCCAGCCAGTTG
CHOP	ATGAACGGCTCAAGCAGGAA	GGGAAAGGTGGGTAGTGTGG
HERPUD1	AACGGCATGTTTTGCATCTG	GGGGAAGAAAGGTTCCGAAG
ATF4	TCCAACAACAGCAAGGAG	ATGGTTTCCAGGTCATCTATAC
XBP1 (total)	TAGCAGCTCAGACTGCCAGA	CCAAGCGCTGTCTTAACTCC
XBP1s (spliced)	GCTGAGTCCGCAGCAGGT	CTGGGTCCAAGTTGTCCAGAAT
SARS-CoV-2 ORF1ab	CCCTGTGGGTTTTACACTTAA	ACGATTGTGCATCAGCTGA
Hamster GAPDH (BHK21)	GCACAGTCAAGGCTGAGAA	GCCAGTAGACTCCACAACATAC
Hamster ATF4 (BHK21)	AGCAAAACAAGACAGCAGCCACTA	TTGCCTTACGGACCTCCTCTATCA

555 conjugated secondary antibody. Glass coverslips were mounted on microscope slides using FluoroMount G with DAPI (Thermo Scientific) and visualized at 40× magnification using a Nikon Eclipse Ts2-FL inverted microscope or 63× magnification under water immersion using a Leica Mica confocal microscope.

Cell viability

The viability of A549 cells in the presence of UPR chemical modulators was assessed using the AlamarBlue reagent (Thermo Scientific) according to the manufacturer protocol.

Plaque assay

Huh7 cells were seeded in 12-well plates at 3.5×10^5 cells per well in DMEM containing 10% FBS. Cellular supernatants containing HCoV-229E were serially diluted in serum-free DMEM. Cells were infected with diluted virus at 37 °C for 2 hours. Viral inocula were removed and replaced with plaquing media (DMEM containing 1.2% carboxymethylcellulose and 2% FBS), and cells were incubated at 33 °C for four days. Cells were fixed and stained using a 0.5% crystal violet solution in 20% methanol to visualize plaques.

Statistical analysis

Statistical analyses were conducted using GraphPad Prism 10 version 10.5.0.

Results

Thapsigargin inhibits HCoV-229E RNA replication

Recently, Tg (Fig. 1A) has been shown to possess potent and broadly acting antiviral activity against several unrelated viruses, including human coronaviruses.[2] To confirm the inhibitory effect of Tg against HCoV-229E in our cell model, A549 lung epithelial cells were primed or pre-treated with increasing concentrations of Tg for 30 minutes. Tg was then removed, and cells were washed, prior to infection with HCoV-229E. The effect of Tg on viral replication and viral titer was assessed 48 hours later. Tg dose-dependently decreases both HCoV-229E intracellular N gene expression (Fig. 1B) and viral titer (Fig. 1C). Additionally, A549 cells were primed with Tg and infected with a HCoV-229E Renilla luciferase (RLuc) reporter virus to determine the effect of Tg on viral protein (RLuc) expression and cell viability (Fig. 1D). We show that Tg potently inhibits 229E-RLuc expression with a half-maximal inhibitory concentration (IC_{50}) of 5 nM, as measured by luciferase reporter activity, without affecting cell viability at the tested concentrations (Fig. 1D). We also confirmed that A549 cell viability was not significantly affected by Tg pre-treatment in the absence of HCoV-229E infection (Fig. S1A). Furthermore, at 48 hours post-infection (hpi) in A549 cells, HCoV-229E infection on its own does not significantly impact cell viability (Fig. S1B).

To identify the replication step(s) that are inhibited by Tg, we performed a time-of-addition assay, in which A549 cells were treated with Tg for 30 min at various time points post-infection (Fig. 1E). Tg most effectively inhibits viral N gene expression when added prior to 12 hours post-infection (Fig. 1E). It still has an antiviral effect when added 4–8 hours post infection, but the antiviral activity begins to wane if added around 8–12 hours post-infection. Since transcription and RNA replication is expected to begin in this time window,[14] we investigated the effect of Tg on the accumulation of HCoV-229E mRNA transcripts and double-stranded RNA (dsRNA) replication intermediates. Tg treatment blocks viral gene expression (Fig. 1F) and completely inhibits the accumulation of dsRNA in infected cells at 24 hours post-infection (Fig. 1G). Multi- and single-step viral growth curves also supported an inhibitory effect at the level of RNA replication (Fig. 1H and I). However, the antiviral effect of Tg was reduced when cells were infected at a higher MOI (Fig. 1I), which could reflect viral antagonism of host pathways involved in the antiviral activity of Tg. Overall, these findings suggest that Tg inhibits HCoV-229E predominantly by blocking viral RNA replication.

Thapsigargin expedites activation of the UPR during HCoV-229E infection

While the antiviral mechanism of Tg is still not fully understood, its ability to induce ER stress and activate the UPR is well documented. Previous studies have suggested that UPR activation by Tg during viral infection may contribute to its antiviral activity.[15–17] In this study, we aimed to specifically test the role of the UPR in the antiviral activity of Tg against HCoV-229E infection. The UPR is comprised of three distinct signalling pathways, each initiated by a corresponding ER resident transmembrane protein (IRE1, PERK, or ATF6) (Fig. 2A). To confirm that Tg activates all three branches of the UPR in A549 cells, we primed cells with Tg for 30 minutes, then washed the cells and added normal media without Tg. We assessed expression of UPR-associated genes representative of each pathway over time (Fig. 2B). Induction of XBP1, CHOP, and HERPUD1 gene expression were used as proxies for IRE1, PERK, and ATF6 pathway activation, respectively. Tg robustly activates each pathway at earlier time points, and expression of ER stress-associated genes was still elevated after 48 h in Tg-primed cells (Fig. 2B).

During the course of infection, HCoV-229E infection induces ER stress (Fig. 2C), likely due to the manipulation of ER membranes to form viral ROs and the excessive translation and processing of viral glycoproteins. Although CoVs have evolved mechanisms to regulate ER stress responses,[18,19] we hypothesized that induction of ER stress by Tg disrupts the ability of HCoV-229E to regulate these responses. To characterize how Tg affects UPR activation in the context of infection, A549 cells were primed with Tg for 30 minutes, washed, and subsequently infected with HCoV-229E. UPR-associated gene expression was assessed at various time points post-infection with or without Tg priming (Fig. 2C). UPR-associated gene expression is induced earlier in infection (4 and 8 hpi) in cells primed with Tg in comparison to DMSO-treated cells, where infection induces the UPR only at later time points (Fig. 2C). CHOP expression, downstream of PERK pathway activation,

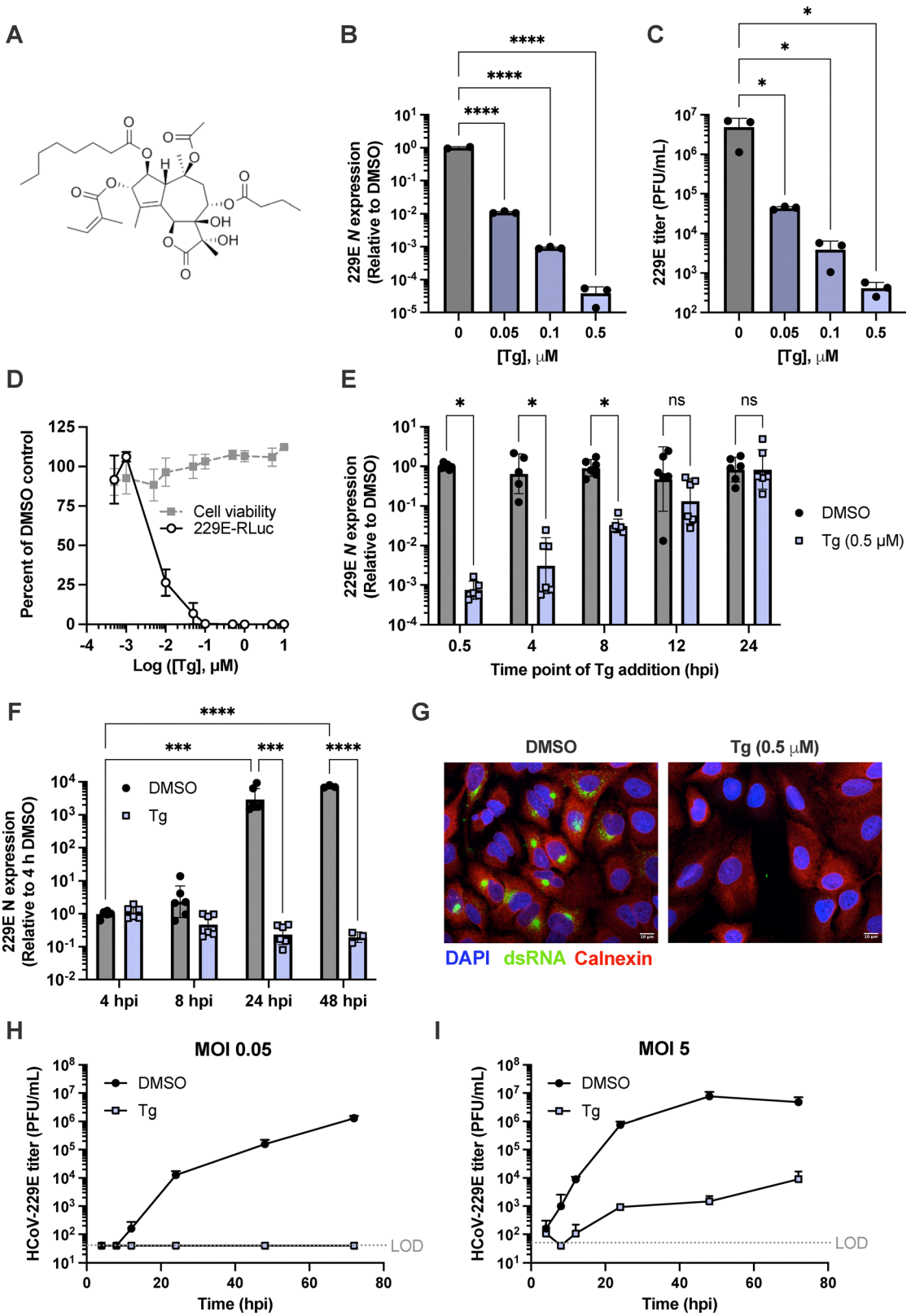

Fig. 1 Tg inhibits HCoV-229E infection during early stages of RNA transcription/replication. (A) Chemical structure of thapsigargin. (B–D) A549 cells were primed with increasing concentrations of Tg for 30 minutes, then washed prior to infection with (B and C) HCoV-229E (MOI 0.01) or (D) a HCoV-229E luciferase reporter virus (MOI 0.5). (B and C) RNA lysates and viral supernatants were collected at 48 hours post-infection (hpi). Viral supernatants were used to assess changes in viral titer *via* plaque assay on Huh7 cells. (D) Luciferase activity was read at 48 hpi as a proxy for viral replication. Alamar blue assay was used to determine the cytotoxicity of Tg in A549 cells. (E) A549 cells were exposed to Tg (0.5 μM) for a 30 minute time period at the indicated time points post infection. RNA lysates were collected at 48 hpi. (F) A549 cells were primed with Tg (0.5 μM) for 30 minutes, then washed prior

to infection with HCoV-229E (MOI 0.05). RNA lysates were collected at the indicated time points post-infection. (B–F) RNA lysates were used to assess changes in gene expression by RT-qPCR. Data are normalized to *18S* gene expression and are expressed relative to DMSO. (G) A549 cells were primed with DMSO or Tg (0.5 μM), then infected with HCoV-229E (MOI 0.5). At 24 hpi, cells were fixed and processed for immunofluorescence, staining for dsRNA (green) and the ER marker calnexin (red) using the appropriate antibodies. (H and I) A549 cells were primed with DMSO or Tg (0.5 μM), then washed and infected with HCoV-229E at low (0.05 pfu per cell) or high (5 pfu per cell) MOI. Supernatants were collected at 4, 8, 12, 24 48 and 72 hpi for titration by plaque assay on Huh7 cells. Graphs show means ± standard deviation from 2–3 independent experiments, with qPCR being performed in technical triplicate. Statistical significance was assessed by one-way or two-way ANOVA (* < 0.05; ***$p < 0.001$, ****$p < 0.0001$).

was induced most strongly, with an approximate 40-fold increase in expression observed in A549 cells primed with Tg, relative to DMSO. These results suggest that Tg expedites the activation of the UPR during HCoV-229E infection, which may contribute to its antiviral effect. We also confirmed that Tg priming inhibits HCoV-229E infection and activates the UPR without affecting cell viability in Huh7 hepatoma cells (Fig. S2A–D), ruling out A549-specific effects.

Since we noticed a prolonged upregulation of UPR-associated genes following Tg priming, we next tested the duration

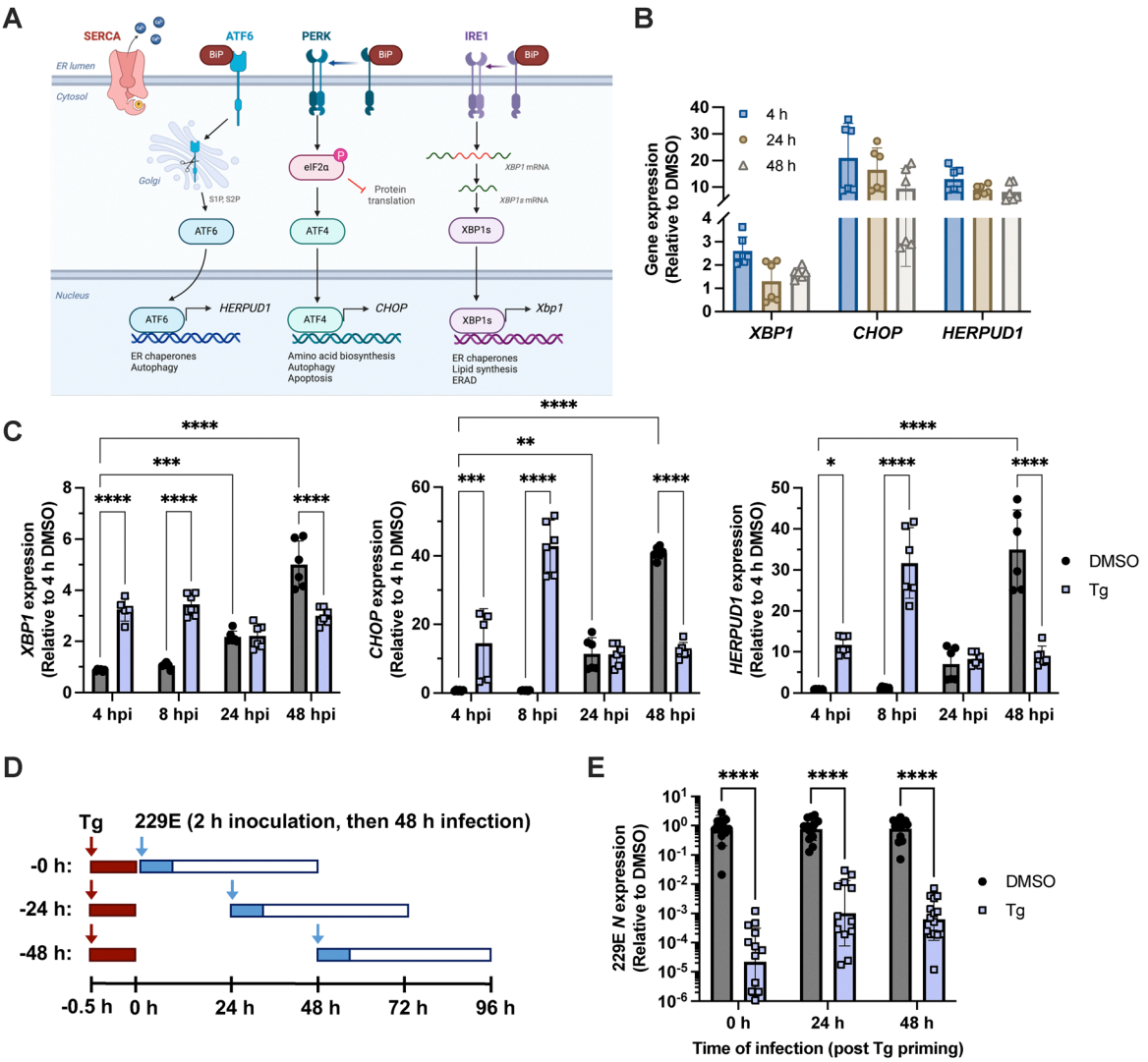

Fig. 2 Thapsigargin broadly activates the UPR and expedites its activation during HCoV-229E infection. (A) Schematic of the ATF6, PERK, and IRE1 arms of the UPR. (B) Cells were primed with Tg (0.5 μM) for 30 minutes, then washed and incubated with normal media. RNA lysates were collected at 4, 24 or 48 h after Tg priming. Expression of UPR-associated genes was assessed by RT-qPCR. (C) A549 cells were primed with DMSO or Tg (0.5 μM) for 30 minutes, then washed and infected with HCoV-229E (MOI 0.05). RNA lysates were collected at 4, 24, or 48 hours after Tg priming. (D and E) Following 30 min of Tg priming, A549 cells were washed and infected with HCoV-229E (MOI 0.05) immediately (0 h), or after 24 or 48 h. RNA lysates were collected at 48 h post-infection. (B–E) Changes in gene expression were assessed by RT-qPCR. Data are normalized to cellular actin and set relative to DMSO. Graphs show mean ± SD from 2–4 independent experiments, with qPCR performed in technical triplicate. Statistical significance was assessed by one-way or two-way ANOVA (*$p < 0.05$, **$p < 0.01$, ***$p < 0.001$, ****$p < 0.0001$).

of its antiviral effect. A549 cells were primed with Tg as described above, and subsequently infected with HCoV-229E at 0 h, 24 h or 48 h post-priming (Fig. 2D and E). Remarkably, Tg retains its antiviral activity and significantly inhibits viral N gene expression, even when cells were infected 48 hours after Tg exposure (Fig. 2E), indicating that the inhibitory effect of Tg is long lasting.

The antiviral activity of Tg against HCoV-229E is not dependent on the individual expression of IRE1, ATF6, or PERK

We next sought to test whether specific pathway(s) of the UPR mediate the antiviral effect of Tg against HCoV-229E infection by stably silencing expression of IRE1, PERK or ATF6 in A549 cells using shRNA (Fig. 3A). A549 shCTRL, shIRE1, shATF6, or shPERK cells were primed with DMSO or Tg for 30 minutes, then washed and subsequently infected with HCoV-229E (MOI 0.05). Tg maintained its antiviral effect against HCoV-229E infection in the knockdown cell lines (Fig. 3B–F), suggesting that Tg does not require the expression of any of these UPR sensors individually to mediate its antiviral effect against HCoV-229E.

We observed that HCoV-229E N protein expression was reduced in the shIRE1 cells in the absence of Tg treatment (Fig. 3B, Fig. S3A), although there were no significant differences at the mRNA level (Fig. 3E). Since Tg priming enhanced IRE1 protein expression in the shIRE1 cells (Fig. 3B and Fig. S3A), we functionally validated IRE1 silencing by assessing Xbp1s expression under these conditions (Fig. S3B). As expected, Tg

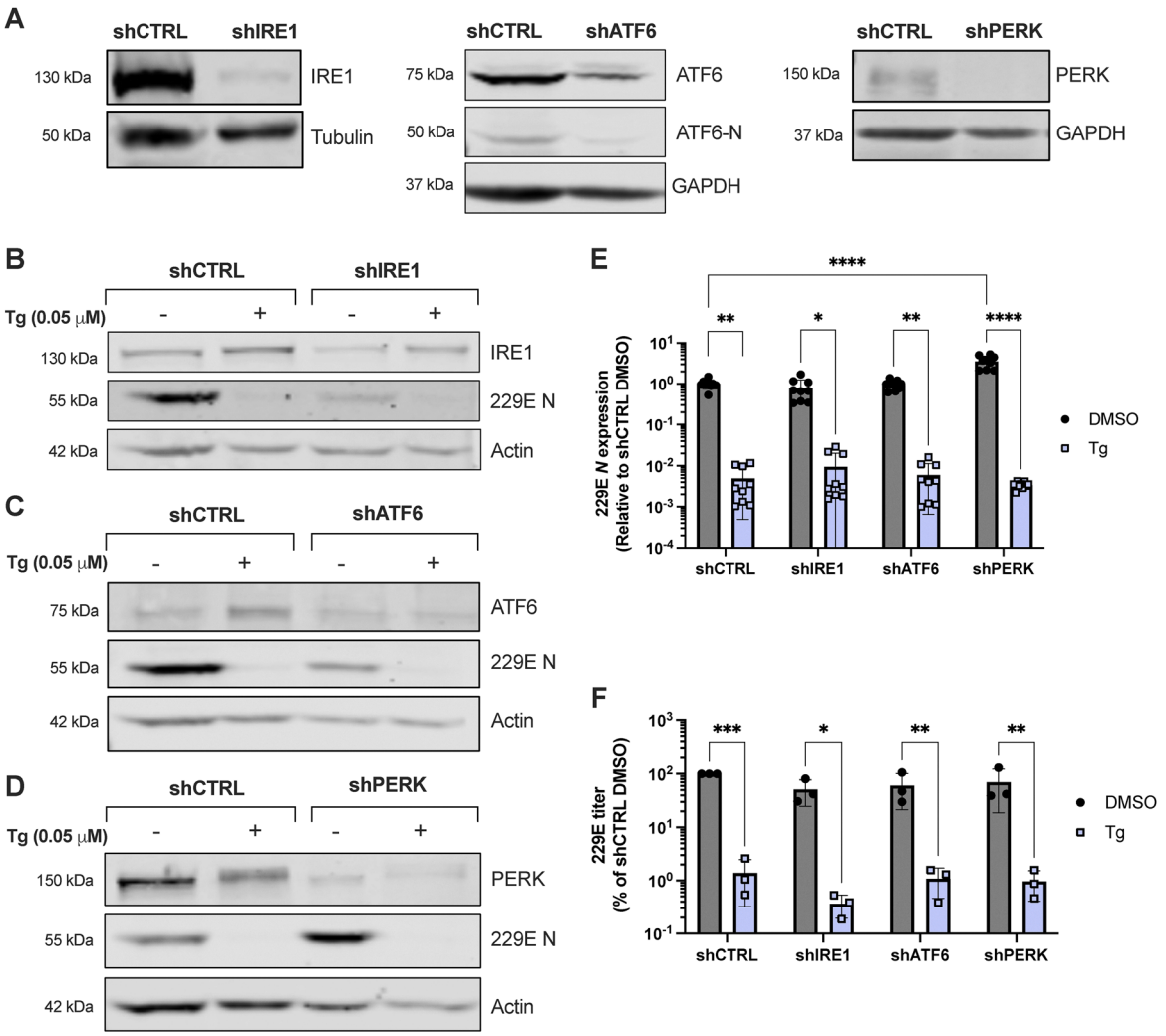

Fig. 3 The antiviral effect of Tg against HCoV-229E infection does not require IRE1, ATF6, or PERK expression. (A) Stable UPR knockdown A549 cell lines were generated *via* lentiviral transduction. Silencing of protein expression was confirmed *via* western blot. (B–F) A549 shCTRL, shIRE1, shATF6, and shPERK cells were primed with DMSO or Tg (0.05 μM) for 30 minutes, then washed prior to infection with HCoV-229E (MOI 0.05). Cell lysates (B–E) or supernatants (F) were collected at 24 hpi. (B–D) Protein expression of IRE1, ATF6, PERK and HCoV-229E N were assessed by western blot. (E) Changes in gene expression were quantified by RT-qPCR. Data are normalized to actin and set relative to shCTRL DMSO. (F) Supernatants were used to determine viral titers by plaque assay on Huh7 cells. Due to variability between replicates, titration data is expressed as a percentage relative to the shCTRL DMSO in each experiment. Graphs show means ± SD from 3 independent experiments, with qPCR performed in technical triplicate. Statistical significance was assessed by two-way ANOVA (*$p < 0.05$, **$p < 0.01$, ***$p < 0.001$, ****$p < 0.0001$).

treatment did not lead to increased Xbp1s expression in the shIRE1 cell line (Fig. S3B). Silencing of ATF6 reduces viral N protein expression (Fig. 3C and Fig. S3C), but did not significantly affect viral mRNA expression. In contrast to our results in the IRE1 and ATF6 knockdown cell lines, HCoV-229E N gene and protein expression is enhanced in the shPERK cells relative to shCTRL cells (Fig. 3D and E and Fig. S3D). These data suggest that PERK restricts HCoV-229E gene and protein expression.

Inhibition of the IRE1 and ATF6 pathways does not impair the antiviral activity of Tg against HCoV-229E

Since residual expression of the UPR sensors in the knockdown cell lines (Fig. 3B–D) could mediate the antiviral effect of Tg, we used pharmacological UPR inhibitors as a complementary strategy to selectively inhibit each pathway. KIRA6,[20] GSK2606414,[21] and Ceapin-A7[22] have previously been shown to selectively inhibit the IRE1, PERK, and ATF6 pathways, respectively. We first confirmed that KIRA6 and Ceapin-A7 inhibit the IRE1 and ATF6 pathway, respectively, by testing their ability to inhibit Tg-induced XBP1s and HERPUD1 protein expression (Fig. 4A and B). Treatment with KIRA6 at its effective concentration reduced cell viability by approximately 50% in A549 cells, while Ceapin-A7 did not significantly affect cell viability, relative to DMSO (Fig. 4C). Unfortunately, the PERK inhibitor GSK2606414 was cytotoxic in A549 cells at all effective concentrations, so we focused on the IRE1 and ATF6 pathways. To further test the role of the IRE1 pathway in HCoV-229E infection and whether it mediates the antiviral effect of Tg, A549 cells were primed with DMSO or Tg alone, or in combination with KIRA6, and then infected with HCoV-229E and incubated in the presence of KIRA6. Co-treatment with KIRA6 significantly inhibits Tg-induced XBP1s expression during infection (Fig. 4D). However, treatment with KIRA6 alone strongly inhibited HCoV-229E replication, making it difficult to assess any further antiviral effect of Tg (Fig. 4E and F). Nonetheless, these findings are consistent with our results in the shIRE1 cell line indicating that activation of the IRE1 pathway by Tg likely does not mediate its antiviral effect against HCoV-229E infection.

To assess the role of the ATF6 pathway, A549 cells were primed with DMSO or Tg in combination with Ceapin-A7 prior to infection (Fig. 4G–I). Ceapin-A7 inhibits Tg-induced HERPUD1 expression during infection, demonstrating its ability to inhibit ATF6 (Fig. 4G and H). However, although Ceapin-A7 alone weakly inhibits HCoV-229E N expression, it does not impair the antiviral effect of Tg against HCoV-229E N gene or protein expression (Fig. 4H and I), ruling out a role for ATF6 pathway activation in the antiviral effect of Tg. Furthermore, co-treatment of infected cells with either KIRA6 or Ceapin-A7 alone, or in combination did not impair the ability of Tg to reduce viral titer (Fig. 4J), further confirming that the IRE1 and ATF6 pathways do not contribute to the antiviral activity of Tg against HCoV-229E infection.

Selective activation of the PERK pathway inhibits HCoV-229E infection

We next used selective pharmacological UPR activators to determine whether activation of UPR pathways alone or in combination mimics the antiviral effect of Tg priming. IXA4,[23] AA147,[24] and CCT020312[25] have previously been shown to selectively activate the IRE1, ATF6, and PERK pathways of the UPR, respectively. We confirmed activation of the respective UPR pathway by treating A549 cells with IXA4, AA147 or CCT020312 for 24 hours. XBP1s (Fig. 5A), HERPUD1 (Fig. 5B), and ATF4 (Fig. 5C) mRNA expression was increased as expected in cells treated with the respective activators. Treatment of A549 cells with IXA4, AA147 or CCT020312 had no effect on cell viability relative to DMSO, although treatment of cells with all three activators in combination reduced cell metabolic activity by approximately 50% as assessed by Alamar blue assay (Fig. S4). Since AA147 and CCT020312 only mildly induced the upregulation of downstream target gene expression (Fig. 5B and C), we confirmed their effects on the UPR at the protein level following 24 h of treatment. AA147 treatment induced upregulation of HERPUD1 protein expression (Fig. 5D), while the effect of CCT020312 on PERK activation was assessed by changes in PERK molecular weight following phosphorylation (Fig. 5E). However, we noted that the effects of AA147 and CCT020312 were less pronounced than that of Tg, reflecting weaker or more transient activation of the UPR compared to the long-lasting and potent effect of Tg (Fig. 5D and E). While AA147 treatment did not affect HCoV-229E N protein expression, CCT treatment decreased HCoV-229E N protein levels (Fig. 5D and E), indicating the antiviral effect of PERK pathway activation.

To further test the effects of the UPR activators on HCoV-229E infection, A549 cells were primed with DMSO or Tg for 30 minutes or treated with the UPR activators for 24 hours following infection with HCoV-229E (Fig. 5F and G). Despite robust upregulation of *Xbp1s* (Fig. 5A), indicating IRE1 pathway activation, A549 cells treated with IXA4 show a very mild reduction in HCoV-229E N gene expression relative to DMSO (Fig. 5F). Furthermore, IXA4 treatment does not significantly affect viral titer (Fig. 5G), supporting our earlier conclusions that activation of the IRE1 pathway likely does not mediate the potent antiviral effect of Tg. Similarly, although treatment of A549 cells with AA147 induces *HERPUD1* expression (Fig. 5D), it had minimal effect on HCoV-229E N gene expression or viral titer (Fig. 5F and G), further supporting that activation of ATF6 does not underlie the antiviral activity of Tg.

Activation of PERK by CCT020312 significantly reduces HCoV-229E N gene and protein expression (Fig. 5E and F), as well as viral titer (Fig. 5G) and somewhat recapitulates the antiviral effect of Tg. To further characterize the antiviral activity of CCT020312 against HCoV-229E infection, we analyzed its effects over a range of concentrations. CCT020312 dose-dependently inhibited HCoV-229E replication, with a potent antiviral effect observed at 10 μM, a concentration at which strong upregulation of CHOP expression, a marker of PERK activation, was observed (Fig. 5H and I). Notably, no significant effects on cell viability were noted at these concentrations (Fig. 5J). These results suggest that selective activation of PERK may at least partially underlie the antiviral effect of Tg.

However, the simultaneous activation of all three pathways of the UPR by treatment with the three UPR activators in combination has a more pronounced antiviral effect (Fig. 5F and G), although does not entirely recapitulate the potency of Tg.

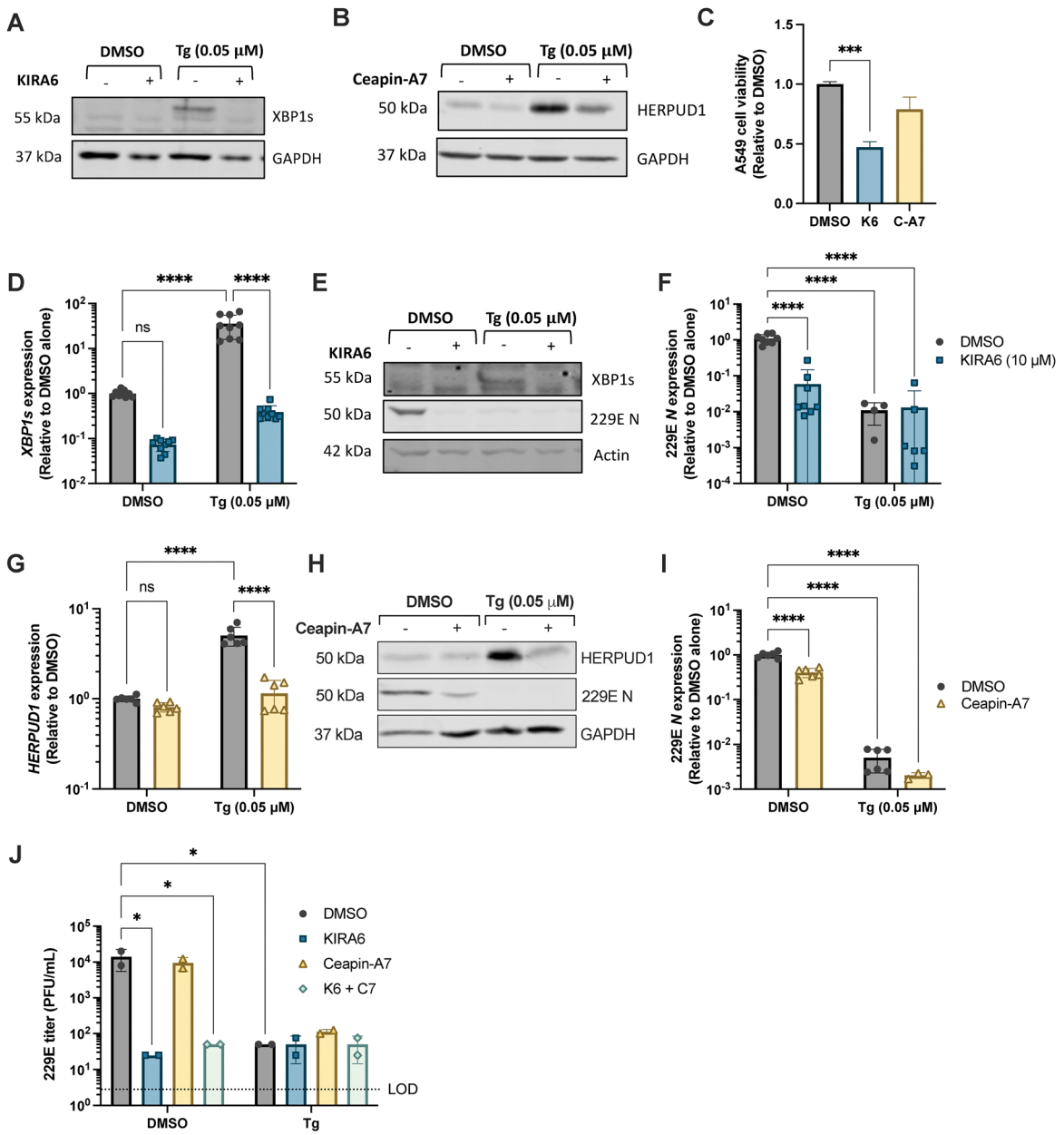

Fig. 4 Pharmacological inhibition of IRE1 or ATF6 does not affect the antiviral activity of Tg against HCoV-229E infection. (A and B) A549 cells were primed with DMSO or Tg (0.05 μM) in the absence or presence of KIRA6 (10 μM) or Ceapin-A7 (6 μM). Cell lysates were collected at 24 hours post-treatment. Xbp1s (A) or HERPUD1 (B) protein expression was assessed by western blot. (C) A549 cells were treated with DMSO, KIRA6 (10 μM), or Ceapin-A7 (6 μM) for 24 hours. Alamar blue assay was used to assess cell viability, which is expressed as a percentage relative to DMSO. (D and F) A549 cells were primed with DMSO or Tg (0.05 μM) in the presence or absence of KIRA6 (10 μM), then washed prior to infection with HCoV-229E (MOI 0.05). Viral inoculum was removed 2 hours later and replaced with media containing DMSO or KIRA6 (10 μM). Cell lysates were collected at 24 hpi to assess *XBP1s* and *N* gene expression by RT-qPCR (D and F), or Xbp1s and HCoV-229E N protein expression by western blot (E). (G and I) A549 cells were primed with DMSO or Tg (0.05 μM) in the presence or absence of Ceapin-A7 (6 μM), then washed prior to infection with HCoV-229E (MOI 0.05). Viral inoculum was removed 2 hours later and replaced with media containing DMSO or Ceapin-A7 (6 μM). Cell lysates were collected at 24 hpi to assess *HERPUD1* and *N* expression by RT-qPCR (G and I), or HERPUD1 and HCoV-229E N protein expression by western blot (H). RT-qPCR data are normalized to actin and set relative to DMSO. (J) A549 cells were primed with DMSO or Tg (0.05 μM) in the presence or absence of KIRA6 (10 μM) or Ceapin-A7 (6 μM), alone or in combination, prior to infection with HCoV-229E (MOI 0.05). Inoculum was removed 2 hours later and replaced with media containing the respective inhibitor(s). Viral supernatants were collected 24 hpi and titrated by plaque assay on Huh7 cells. Graphs show mean ± SD from 2–3 independent experiments performed in triplicate, with qPCR performed in technical triplicate (*$p < 0.05$, ***$p < 0.001$; ****$p < 0.0001$). Representative western blots are shown.

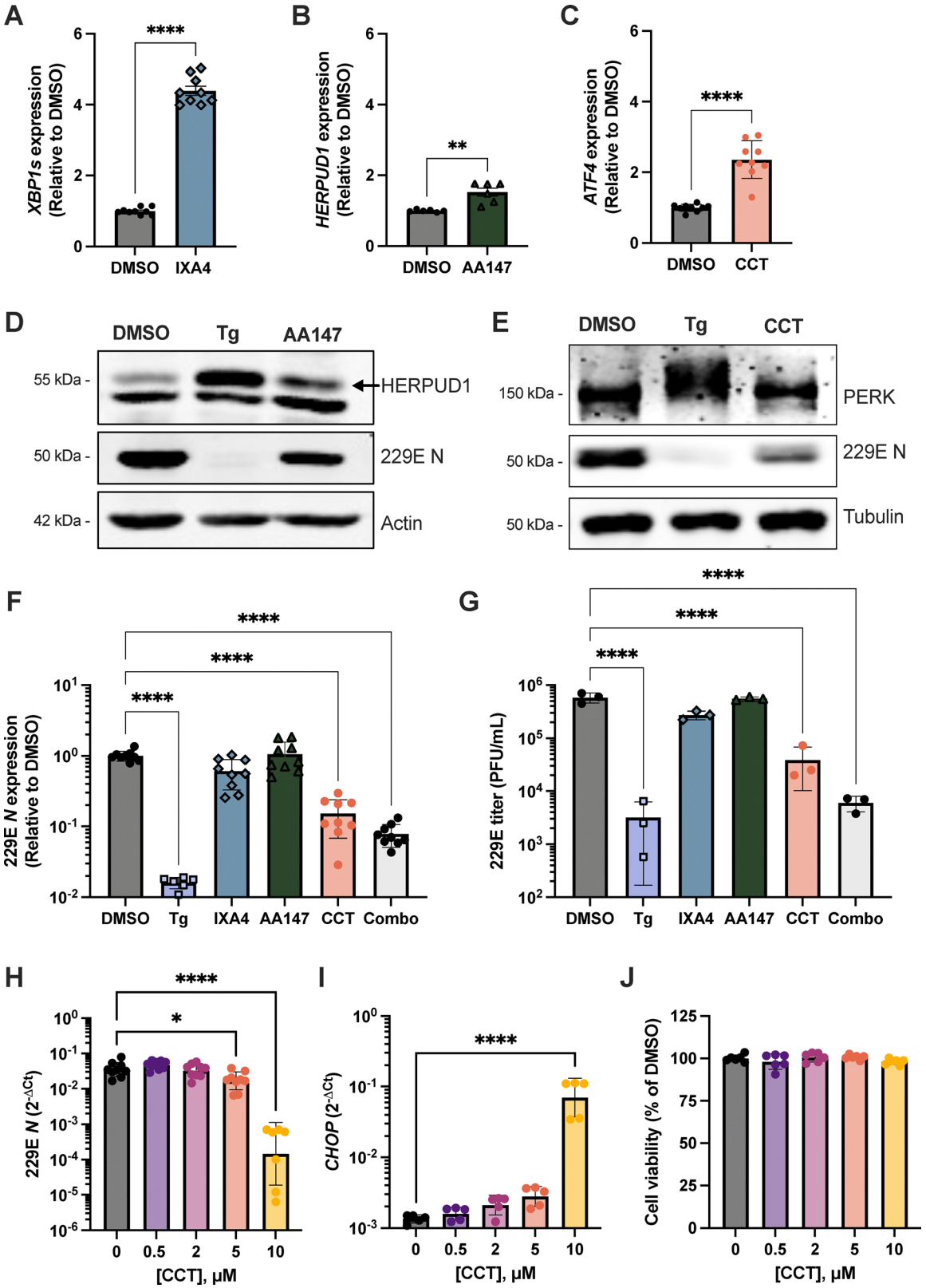

Fig. 5 Pharmacological activation of PERK inhibits HCoV-229E replication. (A–C) A549 cells were treated with DMSO or one of the selective UPR activators for 24 hours. IXA4 (10 μM) activates IRE1, AA147 (10 μM) activates ATF6, and CCT020312 (5 μM) activates PERK. RNA lysates were collected 24 hours post-treatment and the expression of genes downstream of each UPR pathway was assessed by RT-qPCR. Data are normalized to actin and set relative to DMSO. (D) A549 cells were primed with Tg (0.5 μM) for 30 minutes, then washed and infected with HCoV-229E (MOI 0.5). Alternatively, cells were treated with AA147 (10 μM) or CCT020312 (5 μM) for 24 hpi. Cell lysates were collected to assess the expression of HERPUD1, PERK and 229E N

protein by western blot. (F and G) A549 cells were primed with DMSO or Tg (0.05 μM) for 30 minutes prior to infection with HCoV-229E (MOI 0.05). Alternatively, cells were infected and then treated with media containing DMSO or the selective UPR activators alone or in combination. Cell lysates and supernatants were collected at 24 hpi. (F) Changes in HCoV-229E *N* gene expression were assessed by RT-qPCR. Data are normalized to actin and set relative to DMSO. (F) Viral titer was assessed by plaque assay on Huh7 cells. (H–J) A549 cells were infected with HCoV-229E (MOI 0.05), then incubated with increasing concentrations of CCT020312 for 24 h. Cell lysates were collected to assess changes in HCoV-229E *N* gene (H) and *CHOP* (I) expression by RT-qPCR. (J) Cell viability was assessed by Alamar blue assay. Graphs show means ± SD from 2–3 independent experiments performed in triplicate, with qPCR performed in technical triplicate. Statistical significance was assessed by one-way ANOVA or *t*-test (*$p < 0.05$, **$p < 0.01$, ***$p < 0.001$; ****$p < 0.0001$).

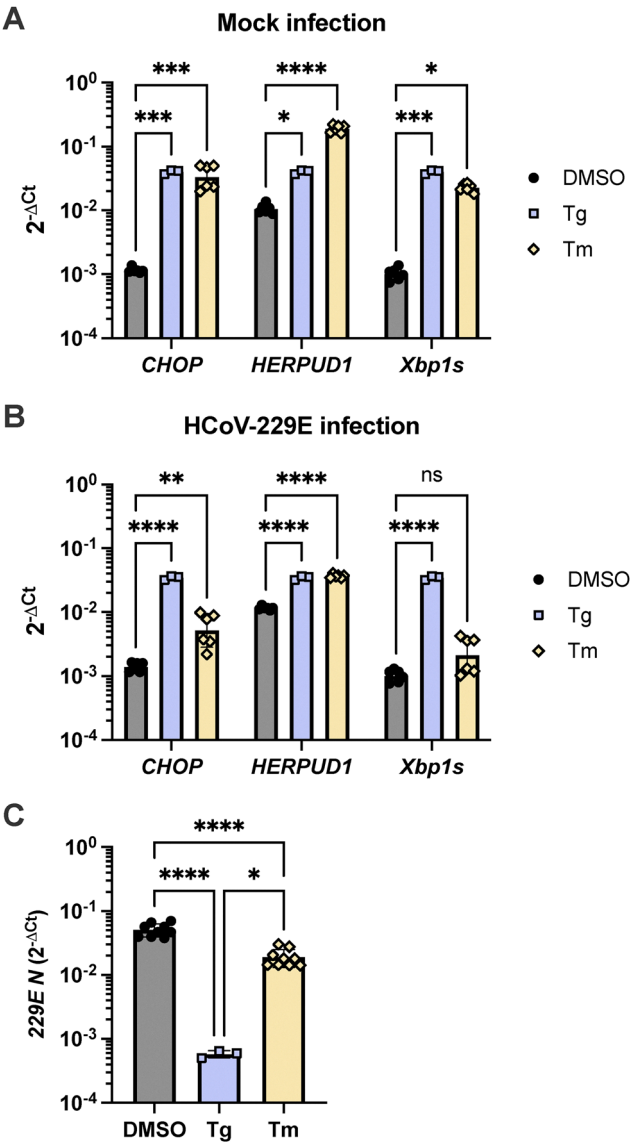

Fig. 6 UPR activation by tunicamycin does not recapitulate the antiviral effect of Tg. (A–C) A549 cells were primed with Tg (0.5 μM) for 30 minutes or with Tm (1 μg mL^{-1}) for 4 hours. Cells were then washed and either mock-infected or infected with HCoV-229E (MOI 0.05). At 24 hpi, cell lysates were collected to evaluate expression of UPR target genes (*CHOP*, *HERPUD1* and *Xbp1s*) or HCoV-229E N gene by qPCR. Graphs show means ± SD from 2 independent experiments, with qPCR performed in technical triplicate. Statistical significance was assessed by one-way or two-way ANOVA (*$p < 0.05$, **$p < 0.01$, ***$p < 0.001$; ****$p < 0.0001$).

UPR activation by tunicamycin does not recapitulate the antiviral effect of Tg

To further probe the role of UPR activation in the antiviral activity of Tg, we used tunicamycin (Tm), which induces ER stress by inhibiting N-linked glycosylation.[26] Pre-treatment of A549 cells with Tg for 30 minutes or Tm (1 μg mL^{-1}) for 4 hours, followed by washing and replacement with normal media, led to robust transcriptional upregulation of UPR target genes 24 hours later (Fig. 6A). In uninfected cells, Tg 30-minute priming and Tm 4-hour priming similarly activated the UPR, with Tm exhibiting a greater effect on ATF6 pathway activation (Fig. 6A). Interestingly, Tm-induced UPR activation was partially antagonized in HCoV-229E-infected cells, while Tg-induced UPR activation was not (Fig. 6B). Tm priming only mildly inhibited HCoV-229E replication (~50% inhibition) in comparison to Tg priming (~2 log inhibition) (Fig. 6C). Thus, Tg-induced UPR activation may be more resistant to viral antagonism, or the antiviral activity of Tg may be partially UPR-independent. Either of these possibilities could explain the more potent antiviral effect of Tg.

Activation of the PERK pathway by CCT020312 inhibits SARS-CoV-2 RNA replication

Since we showed that Tg priming inhibits HCoV-229E RNA replication (Fig. 1), we used a replicon model to evaluate whether Tg priming or selective activation of the PERK pathway by CCT020312 could similarly inhibit the replication of a more pathogenic coronavirus, SARS-CoV-2. We used BHK-21 cells stably expressing a SARS-CoV-2 replicon encoding a nanoluciferase reporter (BHK-CoV-2 cells).[12] BHK-CoV-2 cells were primed with DMSO or Tg, or treated with CCT020312. RNA lysates were collected 24 hours later. Treatment with either Tg or CCT020312 significantly upregulated *ATF4* gene expression, confirming activation of the PERK pathway (Fig. 7A), without significantly affecting cell viability (Fig. 7B). Cells treated with either Tg or CCT020312 show a significant reduction in luciferase activity, a proxy for viral RNA replication, as well as SARS-CoV-2 *ORF1a* gene expression (Fig. 7C and D). Thus, activation of the PERK pathway by CCT020312 inhibits SARS-CoV-2 RNA replication, similarly to Tg. Furthermore, BHK-CoV-2 cells primed with DMSO or Tg, or treated with CCT020312, were processed for confocal microscopy and stained for double-stranded RNA (dsRNA), a viral replication intermediate. Consistently, BHK-CoV-2 cells treated with Tg or CCT020312 have decreased amounts of dsRNA (Fig. 7E). These findings further support our conclusion that Tg priming inhibits CoV RNA

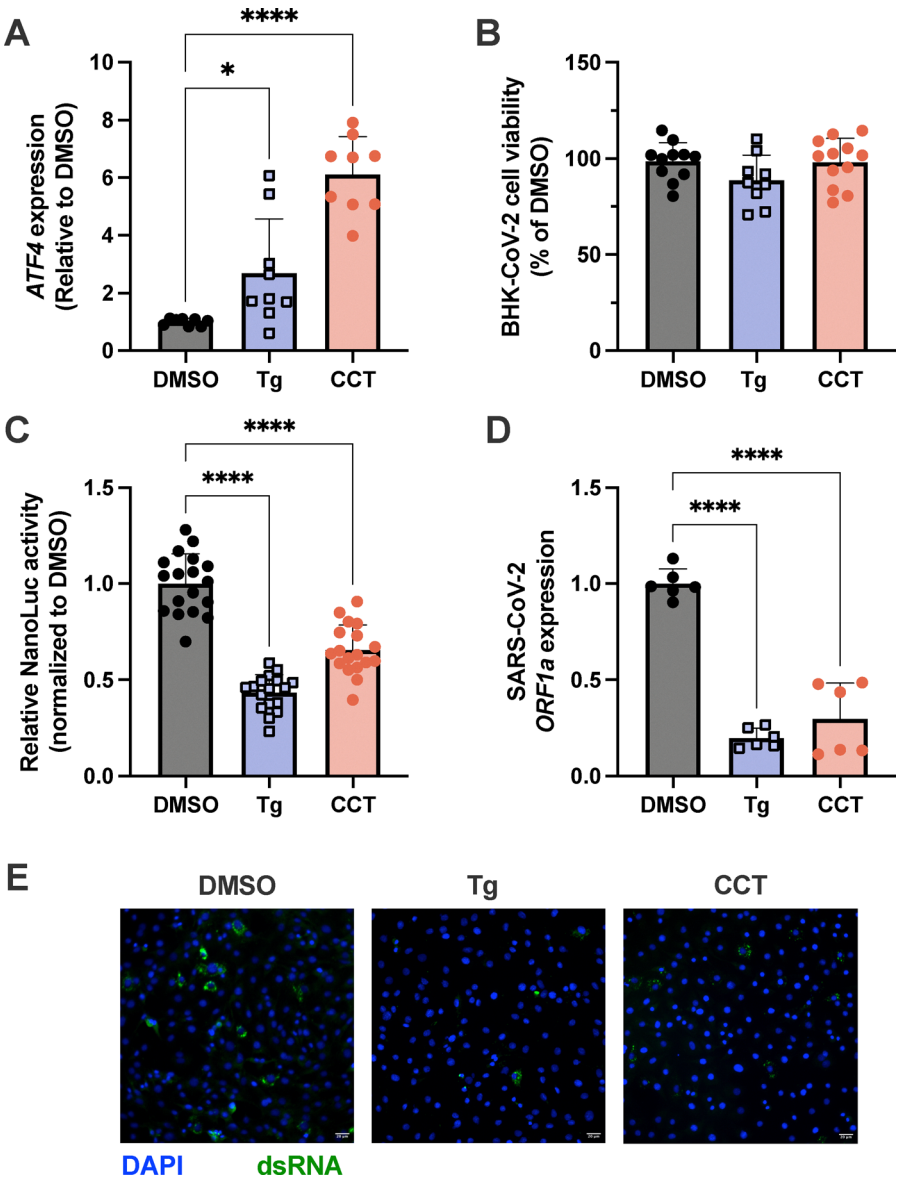

Fig. 7 Selective activation of PERK inhibits SARS-CoV-2 RNA replication. (A–E) BHK-CoV-2 replicon cells were pre-treated with DMSO or Tg (0.5 μM) for 30 minutes, or treated with CCT020312 (5 μM) for 24 h, at which point *ATF4* mRNA expression (A), cell viability (B), and SARS-CoV-2 RNA replication (C and D) were assessed. (A and D) RNA lysates were collected 24 hours post-treatment. Data are normalized to hamster *GAPDH* and set relative to DMSO. (E) BHK-CoV-2 cells were treated with DMSO or Tg (0.5 μM) for 30 minutes, or CCT020312 (5 μM) for 24 hours. Cells were fixed 24 hours later and processed for fluorescence microscopy using an antibody for dsRNA (green). Cells were also stained for DAPI (blue). Graphs show means ± SD from 2–4 independent experiments, with qPCR performed in technical triplicate and NanoLuc measurements performed in technical quadruplicate. Statistical significance was assessed by one-way ANOVA (*$p < 0.05$, ****$p < 0.0001$).

replication. Furthermore, activation of PERK significantly inhibits SARS-CoV-2 RNA replication, suggesting that PERK activation is broadly antiviral against human coronavirus infection.

Discussion

Tg is a potent inducer of ER stress and the UPR, and possesses broadly acting antiviral activity against several unrelated viruses. While literature has shown that Tg inhibits both endemic (HCoV-229E, HCoV-OC43) and pathogenic (MERS-CoV, SARS-CoV-2) human coronaviruses,[2,16] its antiviral mechanism is not fully understood. In this study, we sought to characterize the role of the UPR in mediating the antiviral effect of Tg, using HCoV-229E as a model.

Our data demonstrate that a short 30-minute priming of A549 cells prior to infection with HCoV-229E robustly inhibits viral replication and abrogates the accumulation of viral dsRNA in infected cells (Fig. 1G). Furthermore, our time-of-addition experiments show that a 30-minute treatment with Tg significantly inhibits viral N gene expression when added within the first 8 hours of infection (Fig. 1E), suggesting that Tg exerts its

antiviral effect against HCoV-229E infection by antagonizing early viral RNA synthesis. Consistently, Tg also inhibits SARS-CoV-2 RNA replication in a replicon model (Fig. 7). Like other +ssRNA viruses, CoV RNA transcription and replication occurs within cytoplasmic double-membrane replication organelles (ROs), the formation of which is mediated by viral non-structural proteins (Nsps).[27] The timing of inhibition of viral replication by Tg is consistent with the timing at which the translation of key viral proteins involved in the formation of the CoV replication–transcription complex take place, and the abrogation of dsRNA accumulation in Tg primed cells suggests that the early stages of RNA synthesis are impaired.

Our data show that Tg priming expedites the activation of the UPR in infected cells (Fig. 2C). To test the functional role of each UPR pathway in HCoV-229E infection and the effect of Tg, we used selective pharmacological UPR activators or inhibitors, as well as RNAi. Pharmacological inhibition or genetic knockdown of IRE1, ATF6 or PERK did not affect the ability of Tg to inhibit HCoV-229E gene or protein expression, indicating these UPR pathways individually are not required for the antiviral effect of Tg against HCoV-229E. However, we found that selective activation of the PERK pathway using CCT020312 significantly inhibits HCoV-229E replication (Fig. 5E–J). It is possible that residual expression of PERK in the shRNA cell line may be sufficient to mediate the antiviral effect of Tg. Future experiments in knockout cell lines, or with PERK inhibitors, would help to address this.

The antiviral effect of PERK pathway activation has been shown in the context of another alphacoronavirus, transmissible gastroenteritis virus, where PERK activation during infection negatively regulates viral replication.[28] In addition to the antiviral effect of CCT020312-mediated PERK activation against HCoV-229E infection, we also show that treatment of BHK21-CoV-2 replicon cells with CCT020312 significantly inhibited SARS-CoV-2 RNA replication, providing further evidence that Tg inhibits CoV infection by blocking viral RNA synthesis.

Previous literature shows that CoV infection can activate the PERK pathway. For example, infection with the avian coronavirus infectious bronchitis virus induces the expression of downstream effectors of PERK pathway activation, including CHOP, at 24–48 hpi.[29] The PERK pathway is also activated during SARS-CoV and MERS-CoV infection by the SARS-CoV spike[30] and MERS-CoV membrane[31] proteins, which activate PERK and induce ATF4 and CHOP expression. MERS-CoV infection has been proposed to benefit from PERK-mediated apoptosis.[31,32] Consistently, PERK inhibition reduces MERS-CoV replication in primary lung cells,[31,32] in contrast to our results showing that PERK activation has an inhibitory effect against HCoV-229E or SARS-CoV-2 RNA replication. However, in the case of SARS-CoV-2 infection, only transient PERK pathway activation was observed in infected A549-ACE2 cells, as measured by increases in CHOP expression at 4–8 hpi, but not at later time points,[33] which could reflect viral antagonism of the PERK pathway later in infection.

Activation of PERK could have proviral or antiviral consequences. For example, PERK activation could modulate autophagy and ERAD machinery to support viral RO formation.[34] Additionally, betacoronaviruses, including SARS-CoV-2 and murine hepatitis virus (MHV) can induce autophagy to promote viral egress through the lysosomal pathway.[35] However, the PERK pathway also plays a critical role in regulating host cellular translation through the phosphorylation of eIF2α, leading to the global attenuation of cap-dependent translation. Given that CoVs rely on host cap-dependent translation machinery, many CoVs have evolved strategies to evade host translation shutoff. However, inhibition of eIF2α following Tg-induced PERK activation early in infection could suppress the translation of viral proteins encoding key viral nsps, as well as structural and accessory proteins. As these are required for the assembly of the replication–transcription complex, and antagonism of host responses, this could explain why priming of A549 cells with Tg impairs the transcription of viral mRNAs and the accumulation of viral dsRNA in infected cells. Our data show that Tg priming skews the kinetics and magnitude of PERK pathway activation during CoV infection, which likely contributes to restriction of viral infection.

While activation of the IRE1 pathway did not appear to contribute to the antiviral activity of Tg, we found that treatment of A549 cells with the IRE1 inhibitor KIRA6 strongly inhibits HCoV-229E infection. KIRA6 has been shown to inhibit the phosphorylation of Jun kinases, which could contribute to its observed antiviral effect as JNK kinase regulates phosphorylation of the HCoV-229E nucleocapsid protein.[36] However, IRE1 silencing also led to reduced N protein expression, reflecting previous literature showing that inhibition or genetic knockdown of IRE1 during betacoronavirus HCoV-OC43 or SARS-CoV-2 infection inhibits viral RNA and protein expression and significantly reduces viral titers.[33,37,38] However, other studies have shown that betacoronavirus infection was not affected by genetic knockout of IRE1 or Xbp1s.[39] While the reason for these discrepancies is not clear, one functional consequence of IRE1/XBP1s activation is the induction of ER-associated degradation (ERAD) and the transcription of ERAD-associated genes. ERAD is a quality-control system that facilitates the retro-translocation of misfolded/unfolded proteins out of the ER into the cytosol, tagging them for proteasomal degradation.[40] Several CoVs upregulate ERAD components during infection.[18,34] Interestingly, MHV, a murine betacoronavirus, hijacks EDEMosomes, which are vesicles involved in the transport of ERAD machinery and client proteins from the ER to the lysosome, for use as ROs.[34] While additional experimentation is required to understand the role(s) of the IRE1 pathway during HCoV-229E infection, it is possible that human CoVs may similarly utilize ERAD machinery to facilitate their replication, which could explain why inhibition of IRE1/XBP1s activity reduces HCoV-229E infection. Previous research investigating the role of the IRE1 pathway during coronavirus infection has predominantly focused on betacoronaviruses (SARS-CoV-2, HCoV-OC43, MHV). Our data identifies a similar role for the IRE1 pathway in supporting the replication of alphacoronaviruses, which could be further studied.

Broad perturbation of the UPR by Tg may inhibit CoV infection through a variety of mechanisms.[17] While no individual UPR pathway on its own was required for Tg to exert an antiviral effect, the redundancy and cross-talk between UPR pathways may mask contributions of individual pathways. It is possible that combined activation of all three UPR pathways by Tg may be required for its full antiviral effect. However, robust activation of the UPR by Tm, which causes ER stress by inhibiting *N*-glycosylation, only weakly inhibited HCoV-229E infection (Fig. 6C). It is possible that Tg exerts its antiviral effect(s) against HCoV-229E in a partially UPR-independent manner. Tg potently inhibits SERCA2, thereby disrupting calcium flux and broadly inducing ER stress, which could inhibit viral infection, independently of the UPR. For example, SERCA could be a host factor for HCoV-229E, which could be tested by genetic perturbation of SERCA expression. Alternatively, disruption of host calcium homeostasis by SERCA inhibition could contribute to its antiviral effect. Furthermore, ER stress has been associated with changes in lipid metabolism that could have antiviral effects. A recent study found that Tg and Tm differentially modulate cellular lipid metabolism, with Tg promoting the intracellular accumulation of lipid droplets.[41] Previous studies have also implicated Tg in priming antiviral IFN responses against IAV,[4] as well as flaviviruses including dengue virus and Zika virus.[15] Thus, the antiviral effect of Tg against human CoV infection could be associated with heightened antiviral responses following Tg priming. Further experimentation is required to validate these hypotheses.

Together, our data furthers the understanding of the antiviral mechanism of Tg against human CoV infection. We speculate that Tg-mediated activation of the PERK pathway may contribute to its antiviral effect, since activation of PERK impairs HCoV-229E replication and reduces viral titer, and silencing of this arm of the UPR promotes viral replication. However, the precise mechanisms remain to be elucidated, and the possibility of UPR-independent antiviral mechanisms requires further investigation. Additionally, the use of A549 cells, an adenocarcinoma-derived cell line, in our study is a possible limitation as these cells may respond differently to ER stress. Therefore, in future it will be important to validate these findings in primary human airway epithelial cells.

Conclusion

In summary, our findings provide insight into the antiviral mechanism of Tg against human CoV infection. We show that Tg priming of A549 cells accelerates the activation of the UPR during HCoV-229E infection and inhibits early stages of viral RNA synthesis. While the antiviral effect of Tg does not appear to be dependent on any individual UPR pathway, we show that pharmacological activation of PERK inhibits HCoV-229E infection and SARS-CoV-2 RNA replication. Inhibition of IRE1 potently inhibits HCoV-229E infection, reflecting a proviral role for this arm of the UPR against human coronavirus infection. Overall, we have characterized the role of the UPR in HCoV-229E infection and furthered our understanding of the antiviral mechanism of Tg. These studies could inform the development of host-targeted antiviral strategies to prepare for future emerging CoVs.

Conflicts of interest

There are no conflicts to declare.

Data availability

All the data supporting this article have been included in the main text or in the supplementary information (SI). Supplementary information: Fig. S1. Cell viability following Tg treatment or HCoV-229E infection. (A) A549 cells were treated with the indicated concentrations of Tg for 30 minutes, then washed and incubated in normal media for 48 hours. (B) A549 cells were mock-treated, or treated with DMSO or Tg (0.5 μM) for 30 minutes, then washed and mock-infected or infected with HCoV-229E (MOI 0.05 or MOI 0.5) for 48 h. Cell viability was assessed by Alamar blue assay. Graphs show means ± SD from 2 independent experiments performed in technical triplicate. Statistical significance was assessed by one-way or two-way ANOVA. Fig. S2. Effect of Tg on HCoV-229E infection and UPR activation in Huh7 cells. (A–D) Huh7 cells were primed with DMSO or Tg at the indicated concentrations for 30 minutes, then washed and infected with HCoV-229E. At 24 hpi, cell lysates and supernatants were collected. (A and D) Expression of HCoV-229E N gene or UPR target genes (CHOP, HERPUD1 and Xbp1s) was assessed by RT-qPCR. (B) Extracellular viral titers were determined by plaquing assay on Huh7 cells. (C) Cell viability was assessed by Alamar blue assay. Graphs show means ± SD from 2–3 independent experiments, with qPCR performed in technical triplicate. Statistical significance was assessed by one-way ANOVA (*$p < 0.05$, **$p < 0.01$, ****$p < 0.0001$). Fig. S3. Silencing of UPR sensors and the effect on HCoV-229E protein expression in the presence or absence of Tg. (A–D) Band density analysis was performed in Fiji ImageJ and are expressed relative to the band density ratio obtained in shCTRL DMSO condition. Representative western blots are shown in Fig. S3B–D. (B) Xbp1s expression was evaluated in shCTRL or shIRE1 cells following priming with DMSO or Tg. Graphs show means ± SD from 2 independent experiments. Statistical significance was assessed by two-way ANOVA (*$p < 0.05$, **$p < 0.01$, ***$p < 0.001$). Fig. S4. Cell viability following treatment with UPR activators. A549 cells were primed with Tg for 30 minutes, or treated with the indicated UPR activators (10 μM IXA5; 10 μM AA147; 5 μM CCT020312; or a combination of all three) for 24 h. Cell viability was then assessed by Alamar blue assay and is expressed as percentage relative to DMSO. Graph shows means ± SD from 1–3 independent experiments performed in technical triplicate. Statistical significance was assessed by one-way ANOVA (****$p < 0.0001$). See DOI: https://doi.org/10.1039/d5cb00242g.

Acknowledgements

This work was supported by grants to CCC from the Natural Sciences and Engineering Research Council of Canada (RGPIN-2020-04277) and the Canadian Institutes of Health Research (PTT-184008). We are grateful to the Canadian Foundation for Innovation John R. Evans Leaders Fund (CCC) for equipment that supported this project. THT acknowledges support from a Canada Graduate Scholarship – Master's (CGS-M) and a Vanier Canada Graduate Scholarship. THT and CEGF acknowledge stipend support from the Canadian Network on Hepatitis C. CanHepC is funded by a joint initiative of the Canadian Institutes of Health Research (NHC-142832, NHE-174228, HPC-178912) and the Public Health Agency of Canada. DM and CCC gratefully acknowledge the Bruce Mitchell Research Program at Queen's University for providing stipend support to DM. We are grateful to Dr Craig McCormick (Dalhousie University, Canada) for providing reagents and helpful discussion, and to Dr Volker Thiel (University of Bern, Switzerland) for providing the HCoV-229E-RLuc reporter virus. The following reagents were obtained through BEI Resources, NIAID, NIH: BHK-21 Cell Line Harboring SARS-CoV-2-Replicon (NR-58876), A549 cells (NR-52268) and HCoV-229E (NR-52726).

References

1 V. C. Chitalia and A. H. Munawar, A painful lesson from the COVID-19 pandemic: the need for broad-spectrum, host-directed antivirals, *J. Transl. Med.*, 2020, **18**, 390, DOI: 10.1186/s12967-020-02476-9.

2 S. Al-Beltagi, *et al.*, Thapsigargin Is a Broad-Spectrum Inhibitor of Major Human Respiratory Viruses: Coronavirus, Respiratory Syncytial Virus and Influenza A Virus, *Viruses*, 2021, **13**, 234, DOI: 10.3390/v13020234.

3 M. S. Shaban, *et al.*, Multi-level inhibition of coronavirus replication by chemical ER stress, *Nat. Commun.*, 2021, **12**, 5536, DOI: 10.1038/s41467-021-25551-1.

4 L. V. Goulding, *et al.*, Thapsigargin at Non-Cytotoxic Levels Induces a Potent Host Antiviral Response that Blocks Influenza A Virus Replication, *Viruses*, 2020, **12**, 1093, DOI: 10.3390/v12101093.

5 J. Lytton, M. Westlin and M. R. Hanley, Thapsigargin inhibits the sarcoplasmic or endoplasmic reticulum Ca-ATPase family of calcium pumps, *J. Biol. Chem.*, 1991, **266**, 17067–17071.

6 M. Schröder and R. J. Kaufman, ER stress and the unfolded protein response, *Mutat. Res.*, 2005, **569**, 29–63, DOI: 10.1016/j.mrfmmm.2004.06.056.

7 H. Yoshida, T. Matsui, A. Yamamoto, T. Okada and K. Mori, XBP1 mRNA is induced by ATF6 and spliced by IRE1 in response to ER stress to produce a highly active transcription factor, *Cell*, 2001, **107**, 881–891, DOI: 10.1016/s0092-8674(01)00611-0.

8 D. Scheuner, *et al.*, Translational control is required for the unfolded protein response and in vivo glucose homeostasis, *Mol. Cell*, 2001, **7**, 1165–1176, DOI: 10.1016/s1097-2765(01)00265-9.

9 H. P. Harding, *et al.*, Regulated translation initiation controls stress-induced gene expression in mammalian cells, *Mol. Cell*, 2000, **6**, 1099–1108, DOI: 10.1016/s1097-2765(00)00108-8.

10 H. Nishitoh, CHOP is a multifunctional transcription factor in the ER stress response, *J. Biochem.*, 2012, **151**, 217–219, DOI: 10.1093/jb/mvr143.

11 K. Haze, H. Yoshida, H. Yanagi, T. Yura and K. Mori, Mammalian transcription factor ATF6 is synthesized as a transmembrane protein and activated by proteolysis in response to endoplasmic reticulum stress, *Mol. Biol. Cell*, 1999, **10**, 3787–3799, DOI: 10.1091/mbc.10.11.3787.

12 S. Liu, C. K. Chou, W. W. Wu, B. Luan and T. T. Wang, Stable Cell Clones Harboring Self-Replicating SARS-CoV-2 RNAs for Drug Screen, *J. Virol.*, 2022, **96**, e0221621, DOI: 10.1128/jvi.02216-21.

13 E. V. LeBlanc and C. C. Colpitts, The green tea catechin EGCG provides proof-of-concept for a pan-coronavirus attachment inhibitor, *Sci. Rep.*, 2022, **12**, 12899, DOI: 10.1038/s41598-022-17088-0.

14 M. Cortese, *et al.*, Integrative Imaging Reveals SARS-CoV-2-Induced Reshaping of Subcellular Morphologies, *Cell Host Microbe*, 2020, **28**, 853–866.e855, DOI: 10.1016/j.chom.2020.11.003.

15 T. Carletti, *et al.*, Viral priming of cell intrinsic innate antiviral signaling by the unfolded protein response, *Nat. Commun.*, 2019, **10**, 3889, DOI: 10.1038/s41467-019-11663-2.

16 M. S. Shaban, *et al.*, Thapsigargin: key to new host-directed coronavirus antivirals, *Trends Pharmacol. Sci.*, 2022, **43**, 557–568, DOI: 10.1016/j.tips.2022.04.004.

17 M. Xue and L. Feng, The Role of Unfolded Protein Response in Coronavirus Infection and Its Implications for Drug Design, *Front. Microbiol.*, 2021, **12**, 808593, DOI: 10.3389/fmicb.2021.808593.

18 T. S. Fung, M. Huang and D. X. Liu, Coronavirus-induced ER stress response and its involvement in regulation of coronavirus-host interactions, *Virus Res.*, 2014, **194**, 110–123, DOI: 10.1016/j.virusres.2014.09.016.

19 P. Keramidas, M. Pitou, E. Papachristou and T. Choli-Papadopoulou, Insights into the Activation of Unfolded Protein Response Mechanism during Coronavirus Infection, *Curr. Issues Mol. Biol.*, 2024, **46**, 4286–4308, DOI: 10.3390/cimb46050261.

20 R. Ghosh, *et al.*, Allosteric inhibition of the IRE1α RNase preserves cell viability and function during endoplasmic reticulum stress, *Cell*, 2014, **158**, 534–548, DOI: 10.1016/j.cell.2014.07.002.

21 J. M. Axten, *et al.*, Discovery of 7-methyl-5-(1-[3-(trifluoromethyl)phenyl]acetyl-2,3-dihydro-1H-indol-5-yl)-7H-pyrrolo[2,3-d]pyrimidin-4-amine (GSK2606414), a potent and selective first-in-class inhibitor of protein kinase R (PKR)-like endoplasmic reticulum kinase (PERK), *J. Med. Chem.*, 2012, **55**, 7193–7207, DOI: 10.1021/jm300713s.

22 C. M. Gallagher and P. Walter, Ceapins inhibit ATF6α signaling by selectively preventing transport of ATF6α to

the Golgi apparatus during ER stress, *eLife*, 2016, **5**, e11880, DOI: 10.7554/eLife.11880.

23 J. M. D. Grandjean, *et al.*, Pharmacologic IRE1/XBP1s activation confers targeted ER proteostasis reprogramming, *Nat. Chem. Biol.*, 2020, **16**, 1052–1061, DOI: 10.1038/s41589-020-0584-z.

24 L. Plate, *et al.*, Small molecule proteostasis regulators that reprogram the ER to reduce extracellular protein aggregation, *eLife*, 2016, **5**, e15550, DOI: 10.7554/eLife.15550.

25 S. R. Stockwell, *et al.*, Mechanism-based screen for G1/S checkpoint activators identifies a selective activator of EIF2AK3/PERK signalling, *PLoS One*, 2012, **7**, e28568, DOI: 10.1371/journal.pone.0028568.

26 A. Heifetz, R. W. Keenan and A. D. Elbein, Mechanism of action of tunicamycin on the UDP-GlcNAc:dolichyl-phosphate Glc-NAc-1-phosphate transferase, *Biochemistry*, 1979, **18**, 2186–2192, DOI: 10.1021/bi00578a008.

27 J. Yang, *et al.*, SARS-CoV-2 NSP3/4 control formation of replication organelle and recruitment of RNA polymerase NSP12, *J. Cell Biol.*, 2025, **224**, e202306101, DOI: 10.1083/jcb.202306101.

28 M. Xue, *et al.*, The PERK Arm of the Unfolded Protein Response Negatively Regulates Transmissible Gastroenteritis Virus Replication by Suppressing Protein Translation and Promoting Type I Interferon Production, *J. Virol.*, 2018, **92**, 00431, DOI: 10.1128/jvi.00431-18.

29 Y. Liao, *et al.*, Upregulation of CHOP/GADD153 during Coronavirus Infectious Bronchitis Virus Infection Modulates Apoptosis by Restricting Activation of the Extracellular Signal-Regulated Kinase Pathway, *J. Virol.*, 2013, **87**, 8124–8134, DOI: 10.1128/jvi.00626-13.

30 C. P. Chan, *et al.*, Modulation of the unfolded protein response by the severe acute respiratory syndrome coronavirus spike protein, *J. Virol.*, 2006, **80**, 9279–9287, DOI: 10.1128/JVI.00659-06.

31 H. Chu, *et al.*, Targeting highly pathogenic coronavirus-induced apoptosis reduces viral pathogenesis and disease severity, *Sci. Adv.*, 2021, **7**, eabf8577, DOI: 10.1126/sciadv.abf8577.

32 A. C. Sims, *et al.*, Unfolded Protein Response Inhibition Reduces Middle East Respiratory Syndrome Coronavirus-Induced Acute Lung Injury, *mBio*, 2021, **12**, e0157221, DOI: 10.1128/mBio.01572-21.

33 J. J. Fernandez, *et al.*, The IRE1alpha-XBP1 arm of the unfolded protein response is a host factor activated in SARS-CoV-2 infection, *Biochim. Biophys. Acta, Mol. Basis Dis.*, 2024, **1870**, 167193, DOI: 10.1016/j.bbadis.2024.167193.

34 F. Reggiori, *et al.*, Coronaviruses Hijack the LC3-I-positive EDEMosomes, ER-derived vesicles exporting short-lived ERAD regulators, for replication, *Cell Host Microbe*, 2010, **7**, 500–508, DOI: 10.1016/j.chom.2010.05.013.

35 S. Ghosh, *et al.*, Beta-Coronaviruses Use Lysosomes for Egress Instead of the Biosynthetic Secretory Pathway, *Cell*, 2020, **183**, 1520–1535.e1514, DOI: 10.1016/j.cell.2020.10.039.

36 Y. Bruggemann, *et al.*, JNK kinase regulates phosphorylation of HCoV-229E nucleocapsid protein, *Npj Viruses*, 2025, **3**, 69, DOI: 10.1038/s44298-025-00152-7.

37 J. M. Oda, A. B. den Hartigh, S. M. Jackson, A. R. Tronco and S. L. Fink, The unfolded protein response components IRE1alpha and XBP1 promote human coronavirus infection, *mBio*, 2023, **14**, e0054023, DOI: 10.1128/mbio.00540-23.

38 L. Echavarría-Consuegra, *et al.*, Manipulation of the unfolded protein response: A pharmacological strategy against coronavirus infection, *PLoS Pathog.*, 2021, **17**, e1009644, DOI: 10.1371/journal.ppat.1009644.

39 L. C. Nguyen, *et al.*, SARS-CoV-2 Diverges from Other Betacoronaviruses in Only Partially Activating the IRE1α/XBP1 Endoplasmic Reticulum Stress Pathway in Human Lung-Derived Cells, *mBio*, 2022, **13**, e0241522, DOI: 10.1128/mbio.02415-22.

40 M. H. Smith, H. L. Ploegh and J. S. Weissman, Road to Ruin: Targeting Proteins for Degradation in the Endoplasmic Reticulum, *Science*, 2011, **334**, 1086–1090, DOI: 10.1126/science.1209235.

41 A. Al Otaibi, *et al.*, Thapsigargin and Tunicamycin Block SARS-CoV-2 Entry into Host Cells via Differential Modulation of Unfolded Protein Response (UPR), AKT Signaling, and Apoptosis, *Cells*, 2024, **13**, 769, DOI: 10.3390/cells13090769.